Effect of power quality on the design of proton exchange membrane water electrolysis systems

Koponen Joonas, Ruuskanen Vesa, Hehemann Michael, Rauls Edward, Kosonen Antti, Ahola Jero, Stolten Detlef

DOI: 10.1016/j.apenergy.2020.115791

Effect of Power Quality on the Design of Proton Exchange Membrane Water Electrolysis Systems

Joonas Koponen, Vesa Ruuskanen, Michael Hehemann,* Edward Rauls, Antti Kosonen, Jero Ahola and Detlef Stolten

ABSTRACT

Water electrolyzer technologies may play a key role in the decarbonization of the fossil-fueled world economy. Electrolytic hydrogen production could bridge emission-free power generation and various energy end-use sectors to drive the energy system towards a net zero-emission level. In order to reduce the economic cost of the required energy transition, both the overall system efficiency in converting electrical energy into the chemical energy carried by hydrogen, and the material used to build electrolytic cell stacks, should be optimal. The effect of power quality on the specific energy consumption of proton exchange membrane (PEM) water electrolyzers is investigated with a semi-empirical cell model. An experimentally-defined polarization curve is applied to analyze cell-specific energy consumption as a function of time in the case of sinusoidal current ripples and ripples excited by an industrial 12-pulse thyristor bridge. The results show that the effective electrolyzer cell area should be up to five times as high as an ideal DC power supply when powered by the 12-pulse thyristor rectifier supply to match the specific energy consumption between the two power supply configurations. Therefore, the improvement of power quality is crucial for industrial PEM water electrolyzer systems. The presented approach is applicable to simulate the effect of power quality for different proton exchange membrane electolyzers.

1. Introduction

In the future the entire energy sector must be based on climate friendly technologies. Recently the EU was facing this challenge with presenting a hydrogen strategy [1]. In this context water electrolyzers powered with renewable energy sources may have a very important share in electricity consumption [2]. Large quantities of renewable hydrogen will be needed for seasonal energy storage, to produce carbon-neutral fuels for transportation as well as raw materials for the chemical industry and to serve as combustible in steel or cement industries [3, 4]. The estimated capacity for installed water electrolyzers in a future decarbonized world economy will be in the range of 3,000 to 6,000 gigawatts beyond 2050 as reported in [5]. The estimated scale for required water electrolyzers would make electrolytic hydrogen production the most notable electrical energy consumer in the world [5, 6].

To decrease the cost of renewable-based hydrogen, it is most important to make cheap electricity available and beside that the water electrolyzers specific energy consumption and material use must be minimized [7]. As life cycle assessment has shown that the input energy of PEM electrolysis systems has the main impact on greenhouse gas emissions [8], low specific energy consumption is also beneficial under this aspect. The optimization of the

material used is crucial, especially for the current state-of-the-art PEM water electrolyzers, where iridium is utilized as the catalyst on the anode side.

In the literature the capital expenditure (CAPEX) of Power-to-Gas systems was studied. An important result is that the electrolyzers are the main cost contributors of such systems. The CAPEX of a power converter in a water electrolyzer system is approximately 15% of total CAPEX for both PEM and alkaline water electrolyzer systems [9]. On the other hand, in Mayyas and Mann [10] it is said that power supplies cover 35% of the electrolyzer system cost, but there is no description what is included to the costs in addition to an AC/DC converter – for example transformers, capacitor banks and circuit breakers. The currently increasing production volumes of water electrolyzer manufacturers may affect the price share of water electrolyzer system CAPEX as contract sizes increase to tens and hundreds of megawatts.

The water electrolyzer stack consumes the most of the energy in Power-to-X-systems and hydrogen is the prime energy carrier in the final product [11]. The DC current is supplied to all in series connected cells of the electrolyzer stack and its mean value determines the hydrogen flow of the water electrolyzer. So the cost of electricity determines the main part of the cost for hydrogen gas produced via water electrolysis. Based on the minimum required energy defined by the LHV (lower heating value, for hydrogen = 33.3 kWh kg^{-1}), commercial available alkaline and PEM water electrolyzer stacks can achieve efficiencies between 60 and 71% [12]. Typically the rectifiers used for industrial water electrolyzers are based on thyristors and diodes, as this technology requires high DC currents [13]. Additional heat losses are caused in the electrolyzer due to the thyristors, which are switching with line frequency and generating harmonics on the desired DC-current and DC-voltage [14, 15].

It could be beneficial to applicate more modern power converters based on, e.g., insulated-gate bipolar transistors (IGBTs). Simulation results have shown that the stack-specific energy consumption with a transistor-based converter topology is up to 14% lower in comparison with a 6-pulse thyristor rectifier and up to 9% lower compared with the 12-pulse thyristor rectifier [16]. The efficiency of conventional power converters used in electrolysis systems can reach more than 98%. Therefore optimization of the losses in the converters is secondary compared to the optimization of the stack losses. In other words, decreasing the switching and/or conduction losses in the power converter of the water electrolyzer is still likely to yield far greater benefits for the overall energy efficiency of the water electrolysis system by improving the DC power quality supplied to the electrolytic cells. The thyristor-based rectifier solutions in water electrolyzer systems could be replaced by the pulse-width modulated (PWM) technology extensively used e.g. in solar photovoltaic systems. The main difference for water electrolyzers would be the direction of power flow, which is controlled by software. The current cost for pulse-width modulated PWM power electronics systems in solar photovoltaics is 0.027 EUR/W_p [17]. The cost for PWM power electronics is assumed to decrease further following the learning curve. Furthermore, the use PWM rectifiers would eliminate the need for reactive power compensation equipment on the electricity grid side cutting the related CAPEX and/or OPEX costs compared to thyristor-based solutions.

The effect of dynamic operation has been shown to have effect on PEM electrolyzer degradation rate e.g. in [18, 19]. However, the cycle time of power fluctuation has been in range of seconds or minutes as the power fluctuation caused by power electronics in millisecond range. Thorough study on the effect of power quality on the stack lifetime is still to be conducted.

For this paper, the influence of power quality on the design of PEM water electrolysis systems is analyzed using simulation tools and experimental verification. Both, simulation tools and experimental equipment, have been contributed from LUT and IEK-14 to realize this international study. An experimentally-validated, steady-state

model is presented for PEM water electrolyzer cell voltage, which is then used in simulations of the impact of varying DC current. The selected current waveforms for the analytical investigation are DC with sinusoidal AC ripples and with the waveform generated by a 12-pulse thyristor rectifier bridge typical for high-power, high-current applications. Finally, the simulated effect of the power quality on the specific energy consumption (E_s) of PEM water electrolysis will be discussed. The main contributions of this paper are:

- A steady state model of a PEM electrolysis cell is presented and experimentally-validated.
- The effect of power quality on PEM water electrolyzers is simulated.
- The results offer a practical guideline on how the power quality affects the design of water electrolysis systems.

This paper is structured as follows: Section 2 describes the modeling of the PEM water electrolyzer cell voltage and the efficiency of the electrolyzer. The simulated effects of power quality on PEM water electrolyzers in general are presented in Section 3. Section 4 aims to determine how the specific energy consumption is affected by power quality at selected DC current waveforms with a single PEM water electrolyzer cell.

2. Semi-empirical simulation approach for PEM electrolysis efficiency

The electrical behavior of a PEM electrolyzer cell can be described with a polarization curve that shows the dependence of voltage on current density. A general, relatively easy approach to modeling such a polarization curve was presented by Schalenbach et al. [20] and this is summarized in the following.

2.1. Cell voltage

Important cell voltage-determining effects are shown in Figure 1.

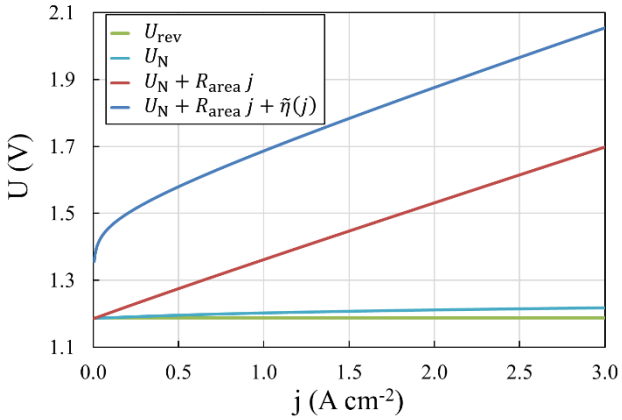

Figure 1. Polarization curve for a typical PEM electrolyzer cell and characteristic contributions to the total cell voltage (according to Schalenbach et al. [20]).

The cell voltage calculation is expressed with:

$$U_{\text{cell}} = U_{\text{N}} + R_{\text{area}}\, j + \tilde{\eta}(j) \qquad (1)$$

where

U_{N} in V is the Nernst Voltage depending on the reversible cell voltage U_{rev},

R_{area} in Ω cm^2 is the sum of all area-specific electrical resistances related to electron and proton transport through all series-connected cell layers,

j in A cm^{-2} is the applied current density, and

$\tilde{\eta}(j)$ in V is the aggregation of activation overpotentials on the anode and cathode sides in a Tafel equation used instead of the more complex Butler-Volmer relationship, which has separate terms and parameters for the anode and cathode.

This approach does not consider further effects such as losses due to gas bubble-blocked catalyst surfaces or a lack of water for the reaction, which may in particular appear at very high current densities (>> 2 A cm^{-2}, see also Smolinka et al. [21]). For a well-designed and advanced electrolysis system operated under nominal operating conditions, these problems should not be relevant. Thus, in the following, the cell voltage is assumed to behave as described in equation (1). Because this approach is semi-empirical, some of the required parameters can be determined with experimental results, as discussed in Schalenbach et al. [22]. Table 1 summarizes all of the equations with an overview of the required parameters to solve (1).

Table 1. Equations used to simulate a polarization curve.

Summand	**Equation**
$U_{\mathrm{rev}} = \frac{1}{2\,F}(-159.6\ \mathrm{J\ mol^{-1}\ K^{-1}})\ T + 2.8472 \cdot 10^5\ \mathrm{J\ mol^{-1}})$ in V where $F = 96485\ \mathrm{As\ mol^{-1}}$ is the Faraday constant and T is the measured cell temperature in K.	*(2)*
$U_{\mathrm{N}} = U_{\mathrm{rev}} + \frac{RT}{2F}\ln\left(\frac{p_{\mathrm{H_2}}}{p_0}\sqrt{\frac{p_{\mathrm{O_2}}}{p_0}}\right)$ in V where $R = 8.31446\ \mathrm{J\ mol^{-1}\ K^{-1}}$ is the gas constant, $p_{\mathrm{H_2}}$ and $p_{\mathrm{O_2}}$ are the partial pressures of hydrogen on the cathode respective of oxygen on the anode side directly at the membrane, both depending on an assumed overpressure in the gas bubbles and the saturated water vapor, as described with (4) and (5), p_0 is the reference, here ambient, pressure (1.01325 bar).	*(3)*
$p_{\mathrm{H_2}} = p_{\mathrm{c}}(j) + \Upsilon_{\mathrm{H_2}} j - p_{\mathrm{sv}}(T)$ in bar $p_{\mathrm{O_2}} = p_{\mathrm{a}}(j) + \Upsilon_{\mathrm{O_2}} j - p_{\mathrm{sv}}(T)$ in bar where $p_{\mathrm{a}}(j)$ and $p_{\mathrm{c}}(j)$ in bar are the measured pressures in the cathode and, accordingly, the anode flow field. $p_{\mathrm{sv}}(T)$ in bar is the pressure of saturated water vapor at the measured cell temperature $\Upsilon_{\mathrm{H_2}}$ and $\Upsilon_{\mathrm{O_2}}$ are the pressure-increasing factors that can be calculated with (6). They represent the current-dependent pressure caused by the gas evolution inside the electrodes on the cathode and anode.	*(4)* *(5)*
$\Upsilon_{\mathrm{H_2}} = \frac{d\frac{AHC}{100\ \mathrm{mol\%}}}{\left(1-\frac{AHC}{100\ mol\%}\right)*4\ F\ \varepsilon_{\mathrm{H_2}}(T)} - \frac{p_{\mathrm{c}}-p_{\mathrm{sv}}(T)}{j}$ in bar $\mathrm{cm^2\ A^{-1}}$ where d in cm is the membrane thickness under wet conditions AHC in mol% is the measured anodic hydrogen content $\varepsilon_{\mathrm{H_2}}(T)$ in mol $\mathrm{cm^{-1}\ s^{-1}\ bar^{-1}}$ is the hydrogen permeability of the membrane at cell temperature.	*(6)*
$R_{\mathrm{area}} = \frac{d}{\kappa\,(T)} + R_{\mathrm{ele}}$ in $\Omega\ \mathrm{cm^2}$ where	*(7)*

$\kappa\ (T)$ in S cm^{-1} is the membrane conductivity at cell temperature R_{ele} in Ω cm^2 is the measured sum of other ohmic resistances (mainly contact resistances between the flow field, PTL and the membrane electrode assembly (MEA)), without the membrane itself.	
$\tilde{\eta}(j) = \alpha \ln(\frac{j}{j_0})$ in V where α is the Tafel slope – also known as the charge transfer coefficient – in V and j_0 in A cm^{-2} is the exchange current density.	*(8)*

2.2. Efficiency

The efficiency of a PEM water electrolysis cell can be expressed as follows:

$$\eta_{\mathrm{cell}} = \eta_{\mathrm{U}}\,\eta_{\mathrm{F}} \qquad (9)$$

where

$\eta_{\mathrm{U}} = U_{\mathrm{rev}}/U_{\mathrm{cell}}$ is the voltage efficiency,

$\eta_{\mathrm{F}} = \frac{j - j_{\mathrm{loss}}}{j}$ is the Faraday efficiency, also known as the current efficiency. For the Faraday efficiency, hydrogen loss is quantified in terms of electric current utilized for its production. In accordance with Schalenbach's approach, the hydrogen losses depend on two effects:

1. Crossover of hydrogen to the anode side, where it can be measured because it is not reacting with the oxygen present at the IrO anode catalyst.
2. Recombination of permeated oxygen with hydrogen to water on the cathode side, which is assumed to react perfectly at the Pt catalyst so that one mole of oxygen consumes two moles of hydrogen.

With these assumptions, the so-called lost current density can be expressed as:

$$j_{\mathrm{loss}} = \frac{2F}{A}(\dot{n}_{\mathrm{H_2per}} + 2\,\dot{n}_{\mathrm{O_2per}}) \qquad (10)$$

where

$\dot{n}_{\mathrm{H_2per}} = \frac{\varepsilon_{\mathrm{H_2}}(T)}{d}\,p_{\mathrm{H_2}}$ is the hydrogen permeation flux, and

$\dot{n}_{\mathrm{O_2per}} = \frac{\varepsilon_{\mathrm{O_2}}(T)}{d}\,p_{\mathrm{O_2}}$ the oxygen permeation flux.

3. Experimental work

3.1. Setup

To obtain characteristic data of a PEM electrolysis cell for the simulation model, the following components were used for the experimental setup at the IEK-14:

Table 2. Experimental setup of the electrolysis cell.

Manufacturer:	Forschungszentrum Jülich, IEK-14
Electrode cathode:	0.39 $\mathrm{mg_{Pt}}$ cm^{-2}
Membrane:	Nafion 117, active area = 17.64 cm^2

Electrode anode:	2.19 mg_{Ir} cm^{-2}
Porous transport layer (PTL) cathode:	Toray paper
PTL anode:	Sintered titanium coated with iridium

The membrane electrode assembly (MEA) was manufactured with a decal process comparable to the method described by Stähler et al. [23]. The cell was operated in a FuelCon electrolyser test rig "C1000-LT Elektroyse" at the IEK-14. This test rig was equipped with an external power supply unit (PSU), provided by LUT [24], and special voltage – respectively current – sensors. These sensors allow high speed ripple measurements. The voltage was measured with the GN840B sensor from HBM and current with a DC current transducer called the "Flux CT600", from the company CAENels. The anodic hydrogen content was measured with the thermal conductivity sensor FTC300 from messkonzept. The cell was supplied with heated water on both, anode and cathode side via gear pumps. The pressures at the cell inlet were measured with "CA 1600 Hydrogen" pressure transmitters from Labom. Figure 2 shows the related P&I diagram.

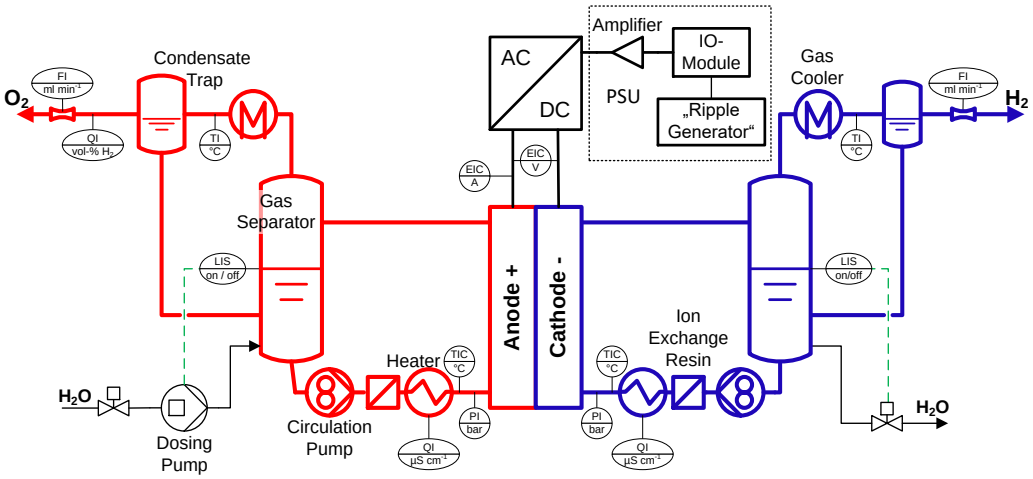

Figure 2. P&I diagram of the used test rig in combination with the LUT ripple generator.

3.2 Measurements

In this study, we concentrated on the measurement of a polarization curve and the anode hydrogen content (AHC) to obtain the main cell-specific parameters. For both measurements, the cell was operated at ambient pressure and with 75 °C, controlled at each cell inlet port (TIC in the P&I diagram). Furthermore, water circulation was realized on both, the anode and cathode sides. The volume flow of water was fixed to 100 ml min^{-1} for both pumps. With this flow the stoichiometric factor regarding the water supply of the cell was varying between 1012 @ 1 A cm^{-2} and 337 @ 3 A cm^{-2} at the anodic cell entrance. Here the stoichiometric factor is defined as the ratio of the circulation molar water flux and the needed molar water flux for the electrochemical reaction. To attain stable cell voltage signals, the current density was varied in steps of five minutes for the polarization curve. The hydrogen crossover was evaluated after the anode hydrogen content signal (AHC, see (6)) was constant for at least 30 minutes.

It was observed that a rising gas evolution leads to a slightly increasing pressure (PI in the P&I diagram) at the anodic and cathodic cell inlet. This effect on the cell pressure is evaluated to describe the current dependency of

p_a and p_c in the simulation model.

Because the cell components, used for this work, have been thoroughly characterized previously the remaining measurable parameters for the semi-empirical simulation model are taken from literature as follows: Ohmic resistance R_{ele} *and* membrane thickness d are taken from [22], membrane conductivity $\kappa(T)$, oxygen and hydrogen permeability $\varepsilon_{H_2}(T)$ and $\varepsilon_{O_2}(T)$ are taken from [20].The following section 3.3 gives an overview of all parameter values.

3.3. Measurement results and parameters for the semi-empirical simulation model

First a polarization curve was measured and then the anodic hydrogen (AHC) content. The measurement results are shown in Figure 3. The observed increase of the pressures at the anode and cathode cell inlet port (p_c *and* p_a) is modelled based on pressure data obtained during the measurement of the polarization curve. The resulting current depending fits for p_c *and* p_a are shown in Table 3. In the next step the AHC (Figure 3 Figure 3. (a) Measured and simulated polarization curve with simulated faraday and voltage efficiency; (b) measured and simulated anodic hydrogen content.(b)) is used for the determination of the pressure increasing factor Y_{H_2}. Contrary to Schalenbach's approach [22], a constant pressure increasing factor Y_{H_2} (6) does not lead to an accurate fitting of the measured AHC. Instead, a precise fitting of $Y_{H_2}$is possible with an additional current-dependent term. In comparison with newer research on hydrogen crossover the resulting equation is correct in meeting the measured AHC, but further aspects of this complex phenomenon are yet to be understood. For example Trinke et al. have reported in [28] that supersaturation of dissolved gas is the best explanation for the current density dependence of the AHC and in [29] Trinke et al. found that also the cathodic ionomer content of the membrane is affecting the AHC. However, the measured and simulated AHC are fitting very well, as can be seen in Figure 3 (b). After $Y_{H_2}$is extracted in that way, Y_{O_2}, $p_{H_2}$and p_{O_2} can be calculated according to equations (4) and (5). With these pressure parameters, the Nernst voltage is calculated, according to equation (3). The cell specific parameters membrane thickness d, membrane conductivity $\kappa\ (T)$ and ohmic resistance R_{ele} are applied in equation (7) to determine the ohmic losses of the cell. The only missing parameters, to model the polarization behavior in equation (1), are Tafel slope α and exchange current density j_0. They can be determined by fitting with the measurement results as shown in Figure 3 (a). Table 3 gives an overview of all parameters, needed for the presented models and the references for data from literatures.

Table 3. Simulation parameters obtained from measurements and the literature.

Parameter	**Value / Equation**	**Unit**	**Source**
T cell temperature	75	°C	Measurement
p_c pressure cathode flow field	$-0.0067\,j^2 + 0.0389\,j + 0.0644$	bar	fitted to measured pressures during polarization
p_a pressure anode flow field	$-0.0109\,j^2 + 0.0474\,j + 0.0383$	bar	
p_{sv} pressure of saturated water vapor	0.3860	bar	[25]
d membrane thickness	0.2100	mm	[22]
κ membrane conductivity	0.1603	S cm^{-1}	[20]

R_{ele} ohmic resistance	0.0290	Ω cm^2	[22]
ε_{H_2} hydrogen permeability	$4.83 \cdot 10^{-11}$	mol cm^{-1} s^{-1} bar^{-1}	[20]
ε_{O_2} oxygen permeability	$2.32 \cdot 10^{-11}$		
γ_{H_2} pressure-increasing factor	$1.2 + \frac{0.3}{j}$	bar cm^2 A^{-1}	fitted with crossover data
$\gamma_{O_2} = ½\ \gamma_{H_2}$	$0.6 + \frac{0.15}{j}$	bar cm^2 A^{-1}	[20]
α is the Tafel slope	0.0253	V	fitted with a polarization curve
j_0 is the exchange current density	$2.641 \cdot 10^{-6}$	A cm^{-2}	

Now, all parameters are known to simulate the behavior of the cell voltage and the anode hydrogen content. The comparison of the simulation results and measurements in Figure 3 demonstrates the high accuracy of the approach used.

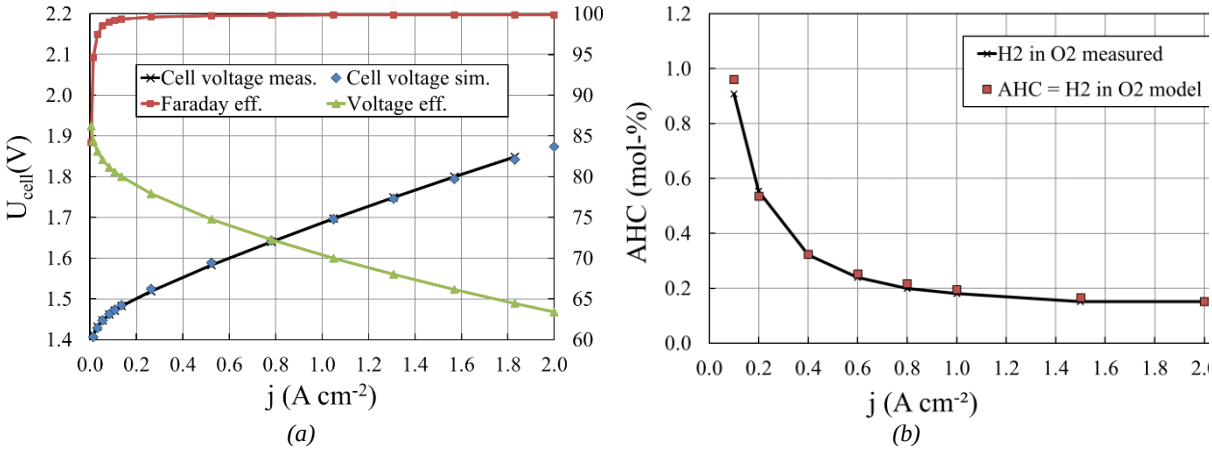

Figure 3. (a) Measured and simulated polarization curve with simulated faraday and voltage efficiency; (b) measured and simulated anodic hydrogen content.

The presented model can be used for the simulation of cell voltages and efficiencies for various ripple scenarios. With some easy measurements, the obtained parameters can also be adjusted to other pressure levels, MEAs or temperatures.

The following example shows the application of the model for a certain ripple scenario. It is assumed that a 300 Hz sine ripple affects the current so that it varies during one period by between 5% and 195% of the nominal current. The resulting cell voltage and efficiency simulation of this sine ripple application can be taken from Figure 4.

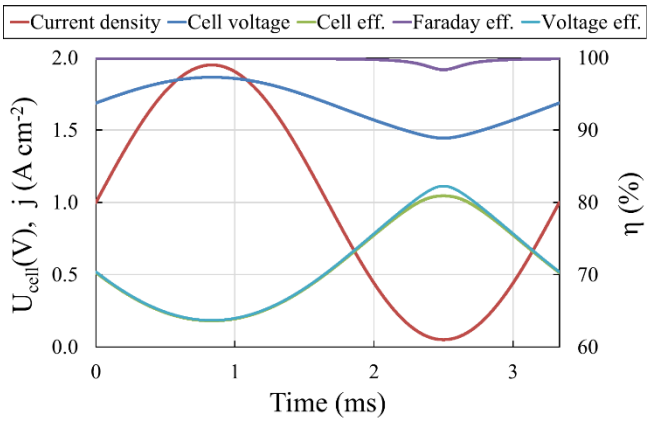

Figure 4. Simulation of cell voltage and efficiencies during one period of a 95% sine ripple on the nominal current @ 300 Hz.

This model can be utilized to assess the theoretical impact of ripple variation on the performance and energy consumption in PEM electrolysis systems. Furthermore, this steady state approach can be used in the future for comparisons with real measurements to evaluate the influence of dynamic effects on cell voltage and efficiency.

The use of steady state voltage−current characteristics assumes that the electrical time constant of the electrolyzer stack is negligible. This assumption is supported by the measurements as nearly no phase shift between voltage and current can be observed at ripple frequency of 300 Hz in Figure 5. Further, because of the lack of liquid electrolyte the dynamics of PEM electrolyzer is often assumed be faster compared with alkaline electrolyzers. However, also the alkaline electrolyzers have been shown to have fast electrical dynamics with current rise time below 1 ms in [26].

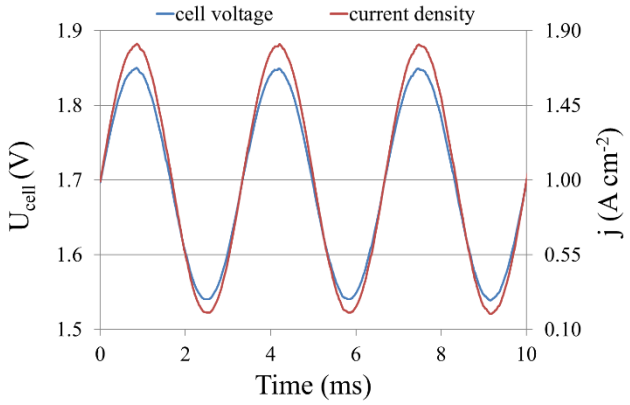

Figure 5. Measured cell voltage and current density during application of 80% sine ripple @ 1.0 A cm^{-2} and 300 Hz.

4 SIMULATION

4.1 Approach

The hydrogen production of an electrolysis cell is directly proportional to the current applied at the electrodes which is described by one of Faraday's laws. The density of the hydrogen production in a single electrolytic cell can be expressed as:

$$f_{H_2} = \eta_F \frac{j\, A\, M_{H_2}}{z\, F} \qquad (11)$$

where

f_{H_2} in g s^{-1} cm^{-2} is the hydrogen production density,

η_F is the Faraday efficiency which is also called current efficiency,

A is the effective cell area in cm^2,

M_{H_2} is the molar mass of hydrogen = 2.016 g mol^{-1} and

z represents the amount of transferred electrons in the reaction (for hydrogen, $z = 2$).

As the momentary electric supply power density of the cell is calculated with the product of the cell current density and voltage, the specific energy consumption E_s can be obtained on the basis of the integration of power density and hydrogen production density for an electrolysis cell. Subsequently for an electrolyzer stack the calculation of the specific energy consumption can be calculated according to Koponen [27]:

$$E_s = \frac{\int_0^{t_1} U_{stack}\, I_{stack} \mathrm{d}t}{\int_0^{t_1} \dot{m}_{H_2}\, \mathrm{d}t} \quad (12)$$

where

E_s is the specific energy consumption in kWh $kg_{H_2}^{-1}$ and

$t1$ is the studied time, which is in this case one full period of the AC ripple.

U_{stack} is the stack voltage

I_{stack} is the stack current

4.2 Results

In the following, 1 p.u. indicates that the AC ripple amplitude equals the DC value and the current density momentarily reaches zero value, which is illustrated in Figure 6.

4.2.1 Sinusoidal current ripple

The first case to be studied is the sinusoidal current ripple. This might not be the case in practical power supplies, but is interesting to investigate, because the ripple is symmetrical above and below the DC value. Figure 5 illustrates a 1 p.u. sine ripple with a 50 Hz frequency (20 ms period) when the DC current is 20 A. 1 p.u. means that the AC current ripple is then ±20 A. Analysis with a sine ripple is now carried out, where the ripple amplitude varies between 0-100% of the DC current density value.

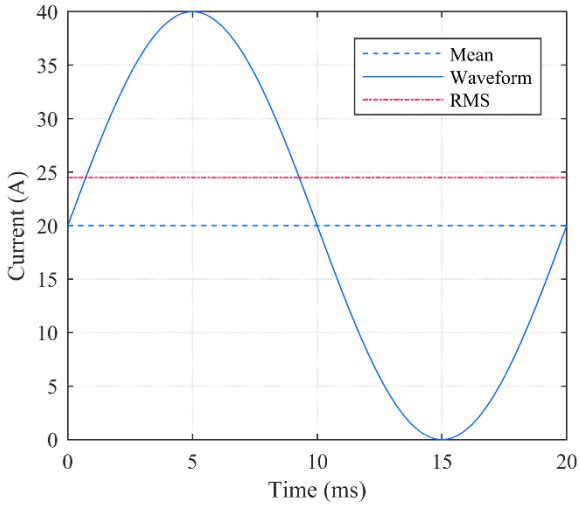

Figure 6. 1 p.u. sine current ripple at a DC current level of 20 A. The mean value and root mean square (RMS) of the DC current waveform are illustrated with dotted lines in blue and red, respectively.

Figure 6 describes the behavior of electrical power as a function of the DC current density and the AC current density ripple. The cell voltage can be determined as a function of time, with the actual ripple-depending current for each time step via (1) based on the current density waveform. Moreover, the power is analyzed point by point, as shown in the nominator of (12).

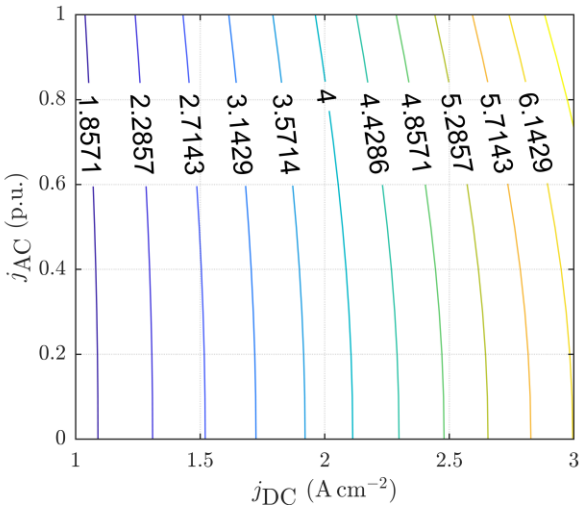

Figure 7. Simulated power density (W m^{-2}) characteristics when the electrolyzer is supplied with DC at increasing levels of sine ripple.

It can be seen from Figure 7 that the power is mainly a function of the current density DC component. However, the AC ripple in the current increases the power consumption, which is emphasized at the highest DC current values. Hydrogen production as a function of the DC and AC current densities is defined in Figure 8 by using (11).

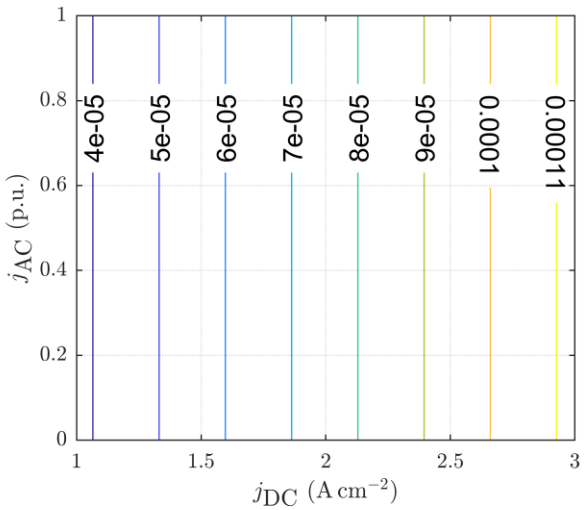

Figure 8. Simulated hydrogen production rate (kg $h^{-1}cm^{-2}$) when the electrolyzer is supplied with DC at increasing levels of sine ripple.

According to Figure 7, the hydrogen production rate is little affected by the current ripple because the average current density (11) remains constant and only the Faraday efficiency varies with the ripple. Hence, it is obvious when comparing Figures 6 and 7 that the current ripple decreases the energy efficiency of the electrolyzer stack. Specific energy consumption is defined by the cell input power and hydrogen production, as shown in (12). The result is shown in Figure 9.

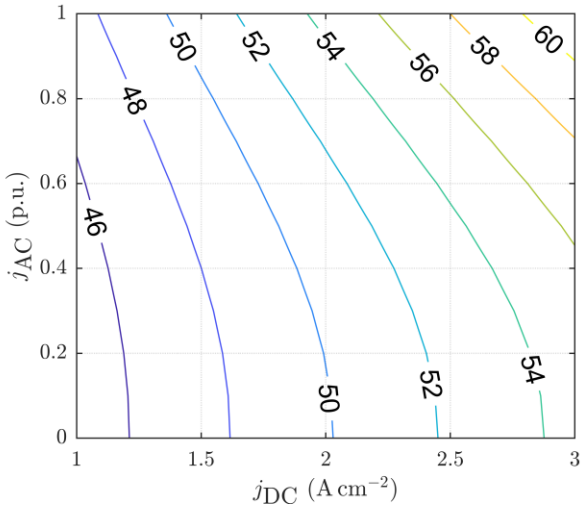

Figure 9. Simulation of the specific energy consumption E_s (kWh $kg_{H_2}^{-1}$) as a function of the current density and current sine ripple.

Figure 8 ensures the result presented above. The effect of the ripple is amplified when the current density is higher. The closer the supplied current is to real DC, the more optimal the E_s of the electrolysis cell is. The lower the current density, the closer the cell voltage is to the Nernst voltage level (see Figure 1). The input power of the supply with ripple power compared to pure DC supply with the same hydrogen production rate is shown in Figure 9. The analysis is repeated with four different DC current densities that are linearly proportional to the hydrogen production rate.

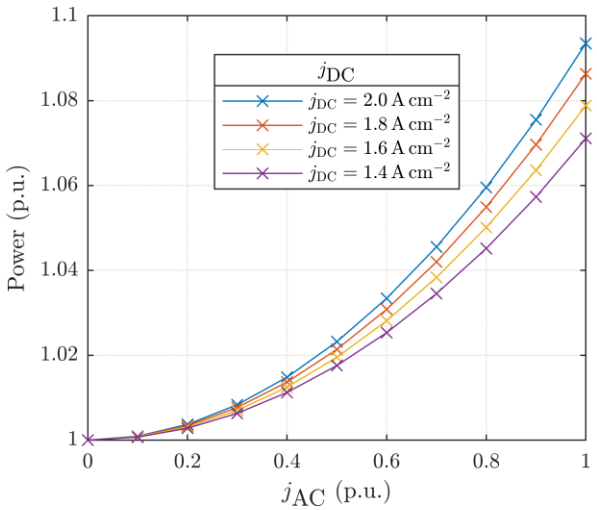

Figure 10. Simulated power consumption as a function of current sine ripple at various DC current densities.

Current ripple has a significant effect on the specific energy consumption (E_s) by generating additional losses. This leads to the fact that the same electrolyzer stack will produce less hydrogen with the same amount of input energy in the presence of current ripple. In other words, increasing the current ripple raises the cost of hydrogen. Therefore, an analysis of compensating the poor power quality by decreasing the current mean value or increasing the cell active area is performed with a sine ripple wherein the ripple amplitude varies 0–100% of the DC current density value.

In the following analysis, a method of E_s-matching is applied to demonstrate the effect of power quality; the ideal DC power supply and the resulting E_s of the PEM water electrolyzer are compared to a non-ideal DC power supply and the respectively resulting E_s of the PEM water electrolyzer as functions of the current density. The E_s-matching method finds the mean current densities that have matching specific energy consumptions. Figure 11 presents the curves for the E_s-matching compared to pure DC currents as sinusoidal ripple is added to the DC supply. Figure 11 also illustrates the required increase in the effective cell area corresponding to the lowered current density to match the E_s and hydrogen production rate with the DC supply: When the AC ripple amplitude equals the DC value (1 p.u.), the required increase in the electrolyzer cell area is +50%. The blue curves in Figure 11 represent constant E_s levels at the designated ideal current density levels.

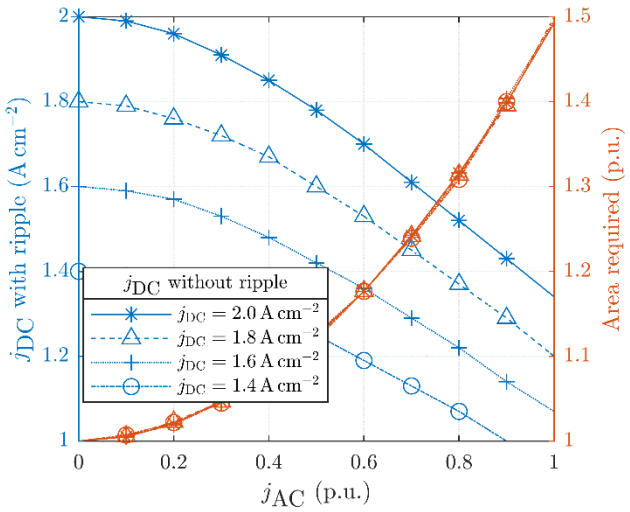

Figure 11. Simulated current lowering with constant specific energy consumption as current ripple is added. The right y-axis presents the effective cell area increase required to compensate for the decreased current if the hydrogen production rate and E_s are kept unchanged.

In other words: If the power quality is improved by decreasing the current ripple, the mean current density may increase while still maintaining the cell E_s level. This means that the current density increase then results in a higher hydrogen production rate with the same electrode area.

4.2.2 Thyristor Bridge (12-Pulse)

The analysis is based on a selection of a range of supply AC voltage levels and firing angles for a thyristor bridge. The AC voltage level and thyristor firing angle define the resulting voltage waveform, as shown in Figure 12. Based on the voltage waveform, the current density can be interpolated with the known polarization curve. Furthermore, the hydrogen production rate and E_s are calculated. The analysis starts with selecting grid voltage and firing angle vectors. Then voltage, current, power and specific energy consumption are analyzed in all combinations. The results below were achieved by selecting the suitable operating points based on the current mean value (hydrogen production) or E_s. The final curves can be smoothed by selecting vectors with smaller steps, leading to longer calculation times.

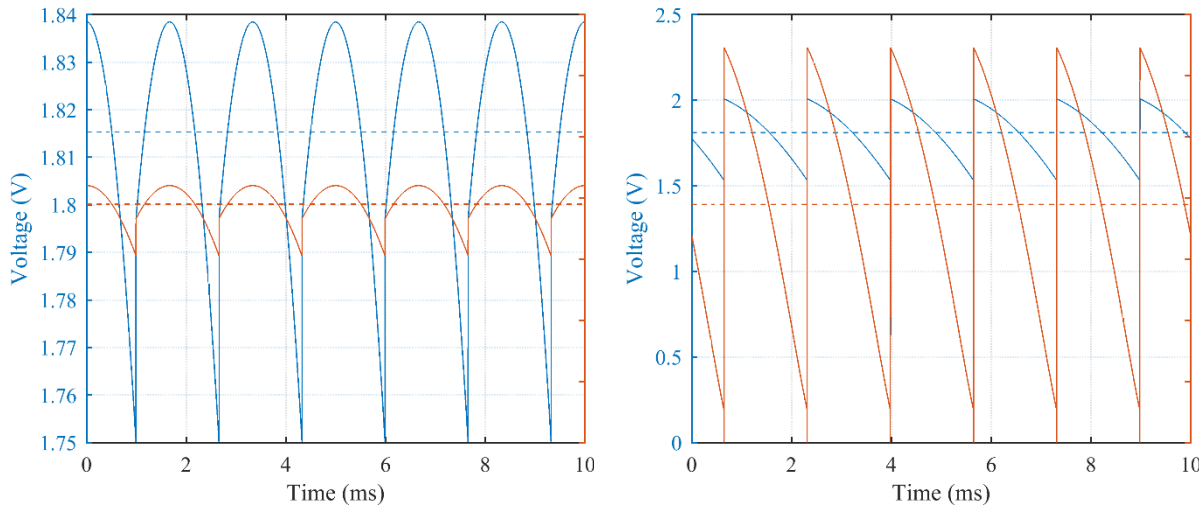

(a) *(b)*

Figure 12. Illustrative 12-pulse thyristor bridge voltage and current waveforms and their mean values with the DC current level of 20 A. The firing angle defines the time instant for the thyristor's turning on. Afterwards, the voltage waveform follows the grid voltage. The current can momentarily reach zero if the voltage is lower than the reversible voltage of the cell. (a) The AC voltage level 1.30 V; (b) the AC voltage level is 1.45 V.

In Figure 13, the supply power with the thyristor bridge is compared to the supply power with pure DC. The firing angle and therefore the current harmonic content are affected by the grid voltage. If the voltage is unnecessarily high, the high firing angle leads to low power quality and higher losses. On the other hand, too low a voltage limits the highest achievable current density at full voltage waveforms.

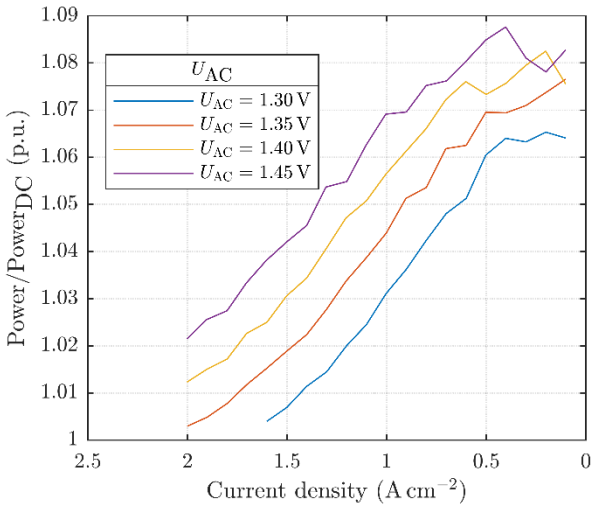

Figure 13. Simulated stack power consumption comparison with thyristor bridge supply at four different AC voltage levels. The stack power consumption with an ideal DC power supply is used as a reference.

In Figure 13, the base value at the *x*-axis is the DC current density. On the left *y*-axis is given the average current density of the thyristor bridge with the E_s-matching the DC value on the *x*-axis. Once again, the grid voltage also affects the results and therefore the analysis is repeated with four grid voltage values. The lowest AC voltage level (1.30 V) cannot output and create a current high enough to reach DC current densities > 1.57 A cm^{-2}. Thus, selecting too low an AC voltage level may limit the current control range; conversely, too high an AC voltage may adversely impact the E_s of the water electrolyzer. On the right y-axis is illustrated the additional area required to compensate the lower current density to match the E_s and hydrogen production with DC. At low current densities close to 0.5 A cm^{-2}, the effective cell area, when powered by the thyristor bridge, must be more than five times larger than with the ideal DC supply to match the hydrogen production rate and E_s.

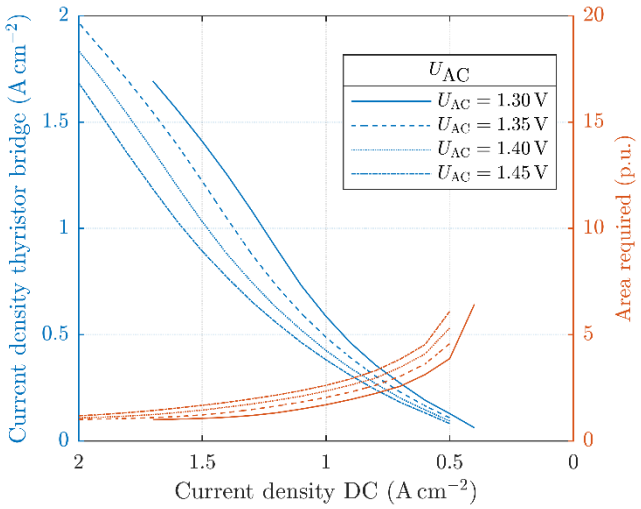

Figure 14. Simulated E_s-matching current lowering with constant specific energy consumption using the thyristor bridge supply at four different AC voltage levels. The x-axis represents the E_s-matching current density with pure DC power supply. The left y-axis presents the E_s-matching mean current density using the thyristor bridge supply, while the right y-axis presents the effective cell area increase required to compensate for the decreased current if both the hydrogen production rate and E_s are kept unchanged.

5. CONCLUSION

A Finish-German cooperation has investigated the effect of current ripple on the proton exchange membrane

water electrolyzer-specific energy consumption using a semi-empirical cell model. This model allows the simulation of the electrolyzer specific energy consumption as a function of time in case of the sinusoidal current ripple and ripple excited by a 12-pulse thyristor bridge. Based on a measured voltage-current characteristic, in conjunction with the anodic hydrogen content measurements at various current densities, all necessary simulation parameters can be determined. To get a concrete example, the method was applied on a single cell with a Nafion 117 membrane. It was found that with the thyristor rectifier supply under the lowest partial loads, the cell area should be up to five times higher than with a pure direct current supply to achieve the same specific energy consumption. It can be concluded that a higher power quality offers lower specific energy consumption. The presented method is applicable for all proton exchange membrane electrolyzers and it helps to find out what is the needed or economically feasible power quality of a concrete electrolysis system. Finally, the authors strongly recommend defining and controlling the maximum current ripple of power converters for the build-up of future sustainable and economic electrolyzer systems.

References

[1] A hydrogen strategy for a climate-neutral Europe. Brussels: European Commission; 2020.
[2] Schmidt PZ, W.; Weindorf, W.; Rakasha, T.; Goericke, D. Renewables in transport 2050 – Empowering a sustainable mobility future with zero emission fuels. 16 Internationales Stuttgarter Symposium. 2016:185-99.
[3] Fasihi M, Bogdanov D, Breyer C. Techno-Economic Assessment of Power-to-Liquids (PtL) Fuels Production and Global Trading Based on Hybrid PV-Wind Power Plants. Energy Procedia. 2016;99:243-68.
[4] Pleßmann G, Erdmann M, Hlusiak M, Breyer C. Global Energy Storage Demand for a 100% Renewable Electricity Supply. Energy Procedia. 2014;46:22-31.
[5] Perner JB, David International aspects of a power-to-xroadmap - A report prepared for the World Energy Council Germany. 2018.
[6] The Future of Hydrogen. Paris: IEA; 2019.
[7] Böhm H, Zauner A, Rosenfeld DC, Tichler R. Projecting cost development for future large-scale power-to-gas implementations by scaling effects. Applied Energy. 2020;264:114780.
[8] Bareiß K, de la Rua C, Möckl M, Hamacher T. Life cycle assessment of hydrogen from proton exchange membrane water electrolysis in future energy systems. Applied Energy. 2019;237:862-72.
[9] Bertuccioli L, Chan A, Hart D, Lehner F, Madden B, Standen E. Study on development of water electrolysis in the EU. 2014.
[10] Mayyas A, Mann M. Manufacturing Competitiveness Analysis for Hydrogen Refueling Stations and Electrolyzers. 2018 Annual Merit Review and Peer Evaluation Meeting: National Renewable Energy Laboratory; 2018.
[11] Vazquez FV, Koponen J, Ruuskanen V, Bajamundi C, Kosonen A, Simell P, et al. Power-to-X technology using renewable electricity and carbon dioxide from ambient air: SOLETAIR proof-of-concept and improved process concept. J Co2 Util. 2018;28:235-46.
[12] Buttler A, Spliethoff H. Current status of water electrolysis for energy storage, grid balancing and sector coupling via power-to-gas and power-to-liquids: A review. Renewable and Sustainable Energy Reviews. 2018;82:2440-54.
[13] Ursúa A, Sanchis P, Marroyo L. Electric Conditioning and Efficiency of Hydrogen Production Systems and Their Integration with Renewable Energies. 2013. p. 333-60.
[14] Ursúa A, Martín IS, Sanchis P. Design of a Programmable Power Supply to study the performance of an alkaline electrolyser under different operating conditions. 2012 IEEE International Energy Conference and Exhibition (ENERGYCON)2012. p. 259-64.
[15] Speckmann F-W, Bintz S, Birke KP. Influence of rectifiers on the energy demand and gas quality of alkaline electrolysis systems in dynamic operation. Applied Energy. 2019;250:855-63.
[16] Koponen J, Ruuskanen V, Kosonen A, Niemela M, Ahola J. Effect of Converter Topology on the Specific Energy Consumption of Alkaline Water Electrolyzers. Ieee T Power Electr. 2019;34:6171-82.
[17] Vartiainen E, Masson G, Breyer C, Moser D, Medina ER. Impact of weighted average cost of capital, capital expenditure, and other parameters on future utility-scale PV levelised cost of electricity. Progress in Photovoltaics: Research and Applications. 2020;28:439-53.
[18] Rakousky C, Reimer U, Wippermann K, Kuhri S, Carmo M, Lueke W, et al. Polymer electrolyte membrane water electrolysis: Restraining degradation in the presence of fluctuating power. Journal of Power Sources. 2017;342:38-47.
[19] Weiß A, Siebel A, Bernt M, Shen TH, Tileli V, Gasteiger HA. Impact of Intermittent Operation on Lifetime and Performance of a PEM Water Electrolyzer. Journal of The Electrochemical Society. 2019;166:F487-F97.
[20] Schalenbach M. Proton conduction and gas permeation through polymer electrolyte membranes during water electrolysis [E-Book]. Jülich: Forschungszentrum, Zentralbibliothek; 2018.
[21] Smolinka T, Ojong ET, Lickert T. Fundamentals of PEM Water Electrolysis. In: Bessarabov D, Wang, H., Li, H., Zhao, N., editor. PEM Electrolysis for Hydrogen Production Boca Raton:. 1st ed. Boca Raton CRC Press; 2015. p. 24.
[22] Schalenbach M, Tjarks G, Carmo M, Lueke W, Mueller M, Stolten D. Acidic or Alkaline? Towards a New Perspective on the Efficiency of Water Electrolysis. Journal of the Electrochemical Society. 2016;163:F3197-F208.
[23] Stähler M, Stähler A, Scheepers F, Carmo M, Stolten D. A completely slot die coated membrane electrode assembly. Int J Hydrogen Energ. 2019;44:7053-8.
[24] Järvinen L, Ruuskanen V, Koponen J, Kosonen A, Hehemann M, Ahola J. Implementing a power source to study the effect of power quality on the PEM water electrolyzer stack. 21st European Conference on Power Electronics and Applications. Genova, Italy2019. p. pp. 1-8.
[25] NIST Chemistry WebBook, Standard Reference Database SRD Number 69.
[26] Ruuskanen V, Koponen J, Sillanpää T, Huoman K, Kosonen A, Niemelä M, et al. Design and implementation of a power-hardware-in-loop simulator for water electrolysis emulation. Renewable Energy. 2018;119:106-15.
[27] Koponen J. Energy effiecient hydrogen production by water electrolysis: Lappeenranta–Lahti University of Technology LUT; 2020.